JOURNAL OF SOLID STATE CHEMISTRY 51, 321–335 (1984)

Structure of Small Oxygen Vacancy Defects in Nonstoichiometric Rutile

L. A. BURSILL

School of Physics, University of Melbourne, Parkville, 3052, Victoria, Australia

AND M. G. BLANCHIN

Departement de Physique des Materiaux, Universite Claude Bernard, Lyon 1 43 Bd du 11 Novembre 1918 69622 Villeurbanne Cedex, France

Received July 18, 1983; in revised form October 7, 1983

New structural models are derived for oxygen vacancy defects, which occur in impurity and dopant-controlled regimes of slightly substoichiometric rutiles. Two reconstructions of the traditional vacancy model are derived, which offer a natural explanation for high-resolution electron paramagnetic (ESR) observations. Both reconstructions involve simply displacement of one cation from (000) to $(-\frac{1}{2}00)$, for a vacancy at $(uu0)$ of the rutile structure. They differ in the distribution of charge-compensating defects associated with the different sites in the immediate vicinity of the defect. Analysis of the electrostatic valencies of the oxygen ions leads to the suggestion that oxygen vacancies in rutile should readily trap H^+ ions. ESR evidence is reviewed offering confirmation of these predictions. Diffusion mechanisms are also described. These new small defect models offer natural explanations for many conflicting interpretations of physical property measurements of reduced and doped rutiles (e.g., electrical conductivity, thermogravimetry, and anelastic dielectric relaxation). The possibility of directly observing and positively identifying such small defects using high-resolution electron microscopic techniques is considered briefly, as is their relevance to the interpretation of plastic deformation and dynamic strain ageing experiments.

1. Introduction

Considerable uncertainty remains concerning the nature of the structural defects responsible for the phase TiO_{2-x} (see, e.g., Akse and Whitehurst (*1*) for a recent literature survey). Most interpretations of physical property and resonance technique measurements have been based upon models for point defect equilibria (see, e.g., Ref. (*2*)). The interpretation of electrical conductivity measurements and of quenching experiments followed by electron diffraction contrast studies (*3, 4*) suggested that for $TiO_{1.9966-2.000}$ the equilibrium phase existing at 1050°C contains no crystallographic shear planes (CSP). Further electrical conductivity studies over a wider range of temperatures (*5, 6*) suggested that there are three domains within TiO_{2-x} (see Ref. (*5*), Fig. 3) where the predominant defects are assumed to be (i) *interstitial* Ti_i^{4+} prevailing for temperature >900°C and for relatively low partial pressures of oxygen (pO_2); (ii) *doubly ionized oxygen vacancies* $V_{\ddot{O}}$, prevailing at lower temperatures and

0022-4596/84 $3.00

for increasing pO_2; with a progressive change to (iii) a second oxygen vacancy defect, initially interpreted as a singly ionized vacancy $V_{\dot{O}}$ (*5*) but later attributed to oxygen vacancies associated with charge compensation of aliovalent Me^{3+} impurities (*6*), prevailing for $x < 0.0016$, regardless of pO_2 or temperature. More recently *in situ* electron microscopic and *ex situ* heating and quenching experiments followed by high-resolution electron microscopic (HREM) observations have revealed some of the details of the mechanisms of formation and dissolution of CSP and other small defects in both reduced TiO_{2-x} and doped $(Ti,Cr)O_{1.98}$ specimens (*7–10*).

In a recent paper new structural models were presented for linear cationic interstitial defects in nonstoichiometric rutile (*11*). These explained many of the features of the HREM images and provided a common structural principle for the range of stoichiometry $TiO_{1.5000-1.999}$, since the new defects consist of pairs of face-sharing octahedra, in common with the CSP. HREM observations of a $TiO_{1.9965}$ specimen, slowly cooled from 1050°C, where the predominant defect should be the cation interstitial, provided convincing evidence for the new interstitial models (*9*).

In this paper it is shown that it is readily possible to derive new structural models for the oxygen vacancy regimes II and III reported by Marucco *et al.* (*5*). These small defects also contain face-shared pairs of octahedra which could, on aggregation after cooling TiO_{2-x} slowly across the phase boundary, precipitate as CSP.

These models readily incorporate foreign ions (or dopants) and offer a natural explanation for many of the difficulties reported in the literature concerning the interpretation of physical property and resonance technique measurements of nonstoichiometric rutile.

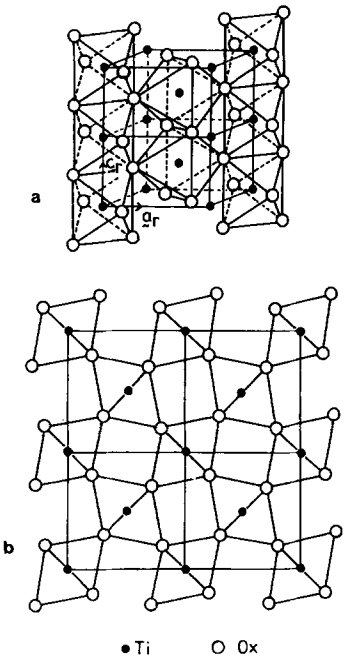

FIG. 1. (a) Perspective view of the rutile structure, showing linkages of almost regular $[TiO_6]$ octahedra. (b) Corresponding [001] pojection of rutile: note location of square tunnels.

2. Derivation of Oxygen Vacancy Structures

(*a*) *Traditional oxygen vacancy structure.* Figure 1a gives a perspective view of the rutile structure,[1] considered as almost regular $[TiO_6]$ octahedra sharing edges, forming columns along [001]. These columns are joined by sharing octahedral corners as shown. Figure 1b shows the corresponding [001] projection. Note especially that each oxygen is shared by three octahedra so that oxygen atoms have triangular plane coordination with respect to the titaniums. The traditional oxygen vacancy model is to simply remove an oxygen ion (Fig. 2a), when there may be some relaxa-

[1] Tetragonal cell $a_r = b_r = 4.5937$ Å; $c = 2.9581$ Å, space group $P4_2/mnm$; Ti at (000, $\frac{1}{2}\frac{1}{2}\frac{1}{2}$); O at ($\frac{1}{2} - u, \frac{1}{2} + u, \frac{1}{2}$; $\frac{1}{2} + u, \frac{1}{2} - u, \frac{1}{2}$; $u, u, 0$; $\bar{u}, \bar{u}, 0$).

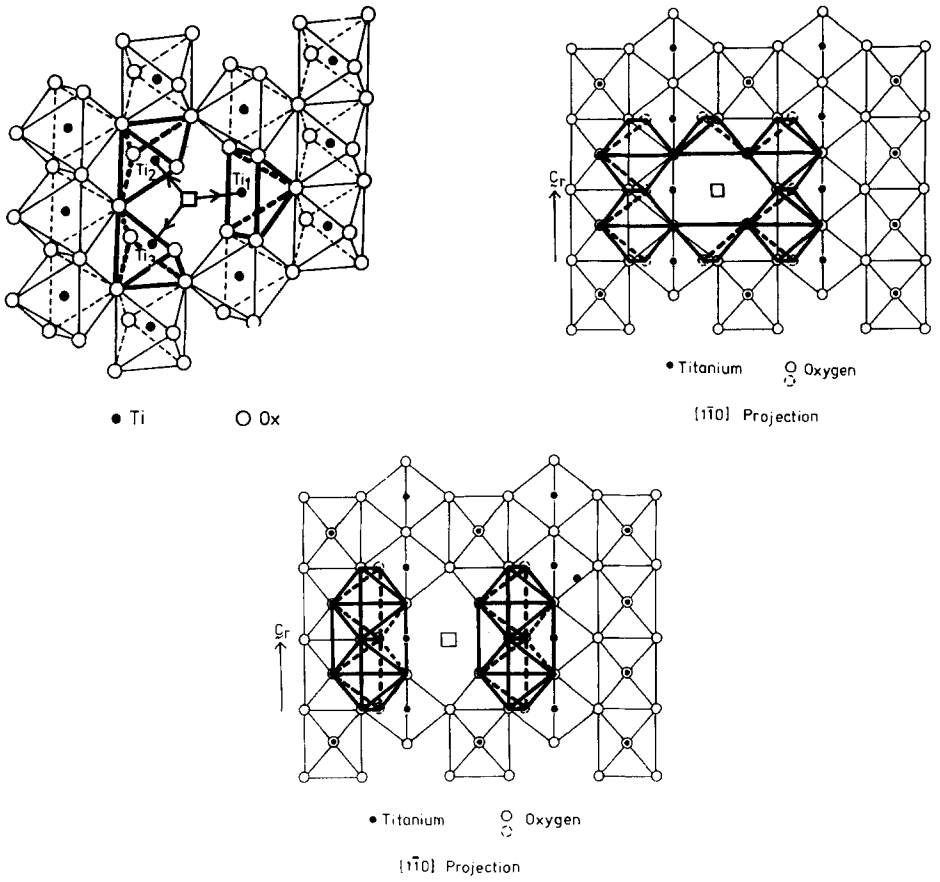

FIG. 2. (a) Oxygen vacancy structure following simple removal of oxygen at ($uu0$). Note triangular coordination of nearest neighbor Ti atoms (Ti_1, Ti_2, and Ti_3), which have distorted square pyramidal fivefold coordination. (b) Showing location of tetrahedral ($\frac{1}{2}0\frac{1}{4}$) [MO_4] interstitial sites adjacent to the oxygen vacancy. (c) Showing location of octahedral ($-\frac{1}{2}00$) [MO_6] interstitial sites adjacent to the oxygen vacancy.

tion of the surrounding three Ti^{4+} cations.[2] Note that after removing an anion the three nearest Ti cations have become five-coordinated to oxygen, one acquiring regular and the remaining two irregular base-centered square pyramidal coordinations. If an oxygen ion is removed from ($uu0$) (Fig. 2a) the three Ti^{4+} ion sites at $Ti_1(000)$, $Ti_2(\frac{111}{222})$, and $Ti_3(\frac{11}{22}-\frac{1}{2})$ are left staring (electrostatically) unshielded at each other. They form an isosceles triangle, having separations 3.57 Å (×2) and 2.96 Å. The corresponding oxygen coordination nearest neighbors are listed in Table I, together with the electrostatic valencies (esv [11]) of the O ions, assuming a doubly ionized oxygen vacancy, with the two equivalent adjacent Ti cations carrying charge +3. Note that there are five oxygens having esv −2.1333, eight with esv = −1.9333 and two with esv = −1.8666. However, the average esv is −2.000 so that the defect is electrically neutral and small shifts of oxygen ions with

[2] Two of these may be (formally) reduced to Ti^{3+} to achieve a neutral charge balance defect. However, the electrical conductivity results suggest (6), at least for T > 800°C, complete ionization of Ti^{3+} ions ($Ti^{3+} \rightarrow Ti^{4+} + e^-$) with consequent delocalization of the electrons.

TABLE I

COORDINATES AND ELECTROSTATIC VALENCIES (ESV) OF OXYGEN IONS ASSOCIATED WITH TRADITIONAL OXYGEN VACANCY MODEL[a]

Ti ion coordinates	O ion coordinate			Σ esv of oxygen ions
(000)	$\frac{1}{2}-u$	$-\frac{1}{2}+u$	$\frac{1}{2}$	−2.1333
($Ti_1 \equiv Ti^{4+}$)	$\frac{1}{2}-u$	$-\frac{1}{2}+u$	$-\frac{1}{2}$	−2.1333
	$-\frac{1}{2}+u$	$\frac{1}{2}-u$	$\frac{1}{2}$	−2.1333
	$-\frac{1}{2}+u$	$\frac{1}{2}-u$	$-\frac{1}{2}$	−2.1333
	$\bar{u}$	$\bar{u}$	0	−2.1333
($\frac{111}{222}$)	$\frac{1}{2}+u$	$\frac{1}{2}-u$	$\frac{1}{2}$	−1.9333
($Ti_2 \equiv M^{3+}$)	$\frac{1}{2}-u$	$\frac{1}{2}+u$	$\frac{1}{2}$	−1.9333
	$1-u$	$1-u$	1	−1.9333
	u	u	1	−1.9333
	$1-u$	$1-u$	0	−1.8666
($\frac{111}{222}$)	$1-u$	$1-u$	0	−1.8666
($Ti_3 \equiv M^{3+}$)	$1-u$	$1-u$	−1	−1.9333
	$\frac{1}{2}-u$	$\frac{1}{2}+u$	$-\frac{1}{2}$	−1.9333
	$\frac{1}{2}+u$	$\frac{1}{2}-u$	$-\frac{1}{2}$	−1.9333
	u	u	−1	−1.9333

Note. If all Ti_i are M^{4+} all Σ esv = 2.1333.

corresponding polarizations will tend to minimize electrostatic energy.

(b) Reconstructed oxygen vacancy structures. The possibilities for recovering more regular coordinations for the three Ti ions adjacent to the oxygen vacancy are now considered. The most obvious sites for interstitial cations in rutile are at ($\frac{1}{2}0\frac{1}{4}$) and ($\frac{1}{2}0\frac{3}{4}$), which lie on each of the vertical faces of the unit cells, and are at the centers of distorted oxygen tetrahedra (Fig. 2b). These sites are joined by a common edge, midpoint ($\frac{1}{2}0\frac{1}{2}$) (Fig. 3a). The latter has a further four (more distant) oxygen neighbors which define a distorted octahedral coordination polyhedron for this interstitial site (Fig. 3b). These octahedral and tetrahedral interstitial sites alternate along the *c*-axis of rutile, forming a continuous tunnel, which is readily apparent in [1$\bar{1}$0] projections of the structure (Figs. 3a and b). The "interstitial" oxygen octahedra (Fig. 2c) are all of the same size and shape, and

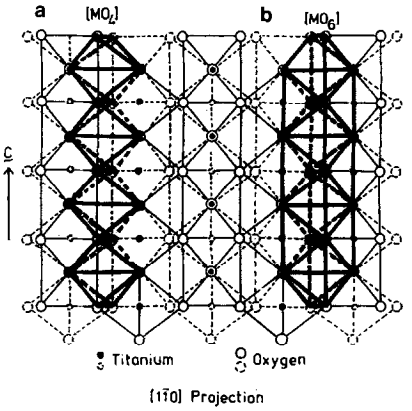

FIG. 3. (a) Showing linkage of $[MO_4]$ tetrahedral interstitial sites along a [001] tunnel. (b) Showing linkage of $[MO_6]$ octahedral interstitial sites along a [001] tunnel. (b) Showing linkage of $[MO_6]$ octahedral intestitial sites along a [001] tunnel. Note relationship to (a).

along the tunnels (or channels) every second one is turned 90° around the *c*-axis and they half-way interpenetrate each other. An interstitial $[MO_6]$ octahedron shares two faces and four edges with neighboring $[TiO_6]$ octahedra. The $[MO_6]$ octahedra differ distinctly from the normal $[TiO_6]$ octahedra, especially in being larger (volume 10.91 Å^3 rather than normal 9.89 Å^3), although they have one very short diameter (=2.66 Å, centered on the two-coordinated site referred to above). The $[MO_4]$ tetrahedral sites lie between $[MO_6]$ octahedral sites (Figs. 3a and b), offering four *M*—O bond lengths of 1.82 Å, which should be compared with the normal Ti—O bond lengths of 1.946 Å (×4) and 1.984 Å (×2). The possibility that some or all of the three Ti ions adjacent to the simple vacancy may occupy either $[MO_6]$ or $[MO_4]$ octahedral or interstitial sites, as a means of recovering much more regular and symmetrical electrostatic environment, must therefore be considered. Such displacements of Ti atoms amount essentially to combination of the traditional vacancy with Frenkel interstitial defects. Energetically we require the "relaxed" or "reconstructed" vacancy to

be lower in energy than the original vacancy. Thus Ti_1 (at 000) may jump to adjacent $[MO_6]$ octahedral sites at $(-\frac{1}{2}00)$ or $(0-\frac{1}{2}0)$. Ti_2 (at $(\frac{111}{222})$) may take octahedral sites at $(1\frac{11}{22})$ or $(\frac{1}{2}1\frac{1}{2})$ whereas Ti_3 (at $(\frac{11}{22}-\frac{1}{2})$) may take octahedral sites at $(1\frac{1}{2}-\frac{1}{2})$ or $(\frac{1}{2}1-1)$. Similarly the corresponding possibilities for tetrahedral $[MO_4]$ sites are Ti_1 (at (000)) moving to $(\pm\frac{1}{2}0\frac{1}{4})$, $(0-\frac{11}{24})$, $(\pm\frac{1}{2}0\frac{3}{4})$, or $(0-\frac{13}{24})$; Ti_2 (at $(\frac{111}{222})$) moving to $(1\frac{11}{24})$ or $(1\frac{13}{24})$ or $(\frac{1}{2}1\frac{1}{4})$ or $(\frac{1}{2}1\frac{3}{4})$; and Ti_3 (at $(\frac{11}{22}-\frac{1}{2})$) moving to $(1\frac{1}{2}-\frac{1}{4})$ or $(1\frac{1}{2}-\frac{3}{4})$ or $(\frac{1}{2}1-\frac{1}{4})$ or $(\frac{1}{2}1-\frac{3}{4})$. The various possibilities for $[MO_6]$ and $[MO_4]$ interstitial sites are listed in Table II. There are in fact many possible reconstructed vacancy structures. Given that there are 7 possible positions for each of Ti_1, Ti_2, and Ti_3, there are already 343 possible structures. Further possibilities arise if Ti ions move to more distant sites.

Displacement of *one* of Ti_1, Ti_2, or Ti_3 into an adjacent $[MO_6]$ site immediately creates one pair of face-shared octahedra

TABLE II

LOCATION OF $[MO_6]$, $[MO_5]$, AND $[MO_4]$ COORDINATION POLYHEDRA IN VICINITY OF OXYGEN VACANCY AT $(uu0)$

Original site	Reconstructed position			Polyhedral nature of site
$Ti_1(000)$	0	0	0	$[MO_5]$ Symmetrical
	$-\frac{1}{2}$	0	0	$[MO_6]$ shares face with $(\bar{1}00)$
	0	$-\frac{1}{2}$	0	$[MO_6]$ shares face with $(0\bar{1}0)$
	$-\frac{1}{2}$	0	$\frac{1}{4}$	$[MO_4]$ shares edges with two normal $[TiO_6]$
	0	$-\frac{1}{2}$	$\frac{1}{4}$	$[MO_4]$ "
	$-\frac{1}{2}$	0	$\frac{3}{4}$	$[MO_4]$ "
	0	$-\frac{1}{2}$	$\frac{3}{4}$	$[MO_4]$ "
$Ti_2(\frac{111}{222})$	$\frac{1}{2}$	$\frac{1}{2}$	$\frac{1}{2}$	$[MO_5]$ asymmetrical
	1	$\frac{1}{2}$	$\frac{1}{2}$	$[MO_6]$ shares face
	$\frac{1}{2}$	1	$\frac{1}{2}$	$[MO_6]$ "
	1	$\frac{1}{2}$	$\frac{1}{4}$	$[MO_4]$ "
	1	$\frac{1}{2}$	$\frac{3}{4}$	$[MO_4]$ "
	$\frac{1}{2}$	1	$\frac{1}{4}$	$[MO_4]$ "
	$\frac{1}{2}$	1	$\frac{3}{4}$	$[MO_4]$ "
$Ti_3(\frac{11}{22}-\frac{1}{2})$	$\frac{1}{2}$	$\frac{1}{2}$	$-\frac{1}{2}$	$[MO_5]$ asymmetrical
	1	$\frac{1}{2}$	$-\frac{1}{2}$	$[MO_6]$ shares face
	$\frac{1}{2}$	1	$-\frac{1}{2}$	$[MO_6]$ "
	1	$\frac{1}{2}$	$\frac{1}{4}$	$[MO_4]$ shares edges
	1	$\frac{1}{2}$	$-\frac{3}{4}$	$[MO_4]$ "
	$\frac{1}{2}$	1	$-\frac{1}{4}$	$[MO_4]$ "
	$\frac{1}{2}$	1	$-\frac{3}{4}$	$[MO_4]$ "

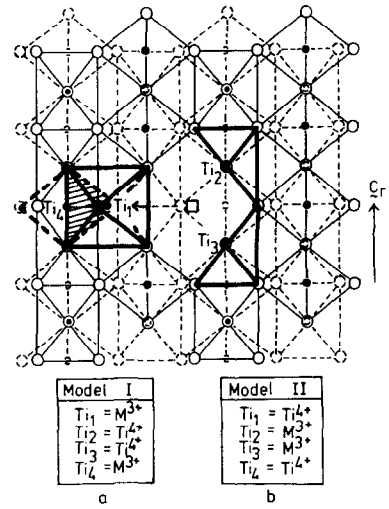

FIG. 4. Showing production of face-shared pair of $[TiO_6]$-$[MO_6]$ octahedra by displacement of Ti_1 (Fig. 2a) by vector $(-\frac{1}{2}00)$. Ti^{3+} charge compensation defects may be placed at either $(-\frac{1}{2}00)$ and (-100) (a) Model I; or, alternatively $(\frac{111}{222})$ and $(\frac{11}{22}-\frac{1}{2})$ (b) Model II.

(Model I; Fig. 4a); e.g. $[MO_6]$ at $(-\frac{1}{2}00)$ shares a face with a normal $[TiO_6]$ octahedron at (-100), leaving (000) vacant. *Note that the oxygen vacancy would lie at second and third nearest neighbor anion sites for M^{3+} at $(-\frac{1}{2}00)$ and (-100), respectively* (cf. discussion of $Cr:TiO_2$ ESR spectra in Section 3 below). *Such a single face-shared pair structural element would allow two M^{3+} ions to be accommodated with the same coordination linkage as occurs in the corundum-type structures* of M_2O_3 (e.g., $M = Ti^{3+}$, Al^{3+}, Fe^{3+}, Cr^{3+}, etc.) and is attractive conceptually in that it forms a unit of M_2O_3-structure coherently intergrown with rutile (Fig. 4a). The latter is the basis of the structural principles involved throughout the crystallographic shear phases Ti_nO_{2n-p} (n,p are integers) occupying the stoichiometry range Ti_2O_3 to $TiO_{1.98}$ (*12*) and also extended recently to the "interstitial" regime of the TiO_{2-x} phase (*12*). This is a very simple modification to the traditional oxygen vacancy model; i.e., a shift of one Ti ion by $(-\frac{1}{2}00)$ and (formally at least) placement of

Ti^{3+} ions at $(-\frac{1}{2}00)$ and (-100). Aggregation of such small defects would readily produce CSP by a vacancy loop partial dislocation mechanism (*13, 14*). The electrostatic valencies generated by this reconstruction are analyzed in Table III. Note that there are two very high values (−1.333) which imply an increase in electrostatic energy compared with the traditional model. In fact these esv values are closer to those expected for OH^- ions (−1.000) than for O^{2-}. It is significant therefore that there is strong evidence from ESR and infrared studies, of both reduced and Fe-doped rutile crystals, that H^+ defects are located at approx. $(\frac{1}{2}00)$ type interstitial sites (see Sections 3 and 4 below).

There is an alternative distribution of M^{3+} ions which should be considered

TABLE III

COORDINATES AND ELECTROSTATIC VALENCIES (ESV) OF OXYGEN IONS ASSOCIATED WITH RECONSTRUCTED VACANCY MODEL I (FIG. 4a)

Coordinates of oxygen ions experiencing changed esv			Σ esv of oxygen ions
$\frac{1}{2}-u$	$-\frac{1}{2}+u$	$\frac{1}{2}$	−1.333
$\frac{1}{2}-u$	$-\frac{1}{2}+u$	$-\frac{1}{2}$	−1.333
$\frac{1}{2}+u$	$\frac{1}{2}-u$	$\frac{1}{2}$	−1.833
$-\frac{1}{2}+u$	$\frac{1}{2}-u$	$-\frac{1}{2}$	−1.833
$\bar{u}$	$\bar{u}$	0	−1.833
$-\frac{1}{2}-u$	$-\frac{1}{2}+u$	$\frac{1}{2}$	−2.333
$\frac{1}{2}-u$	$-\frac{1}{2}+u$	$-\frac{1}{2}$	−2.333
$-1+u$	u	0	−2.333
$-1-u$	$\bar{u}$	0	−1.833
$-\frac{3}{2}+u$	$\frac{1}{2}-u$	$\frac{1}{2}$	−1.833
$-\frac{3}{2}+u$	$\frac{1}{2}-u$	$-\frac{1}{2}$	−1.833
$\frac{1}{2}+u$	$\frac{1}{2}-u$	$\frac{1}{2}$	−2.133
$\frac{1}{2}-u$	$\frac{1}{2}+u$	$\frac{1}{2}$	−2.133
$1-u$	$1-u$	1	−2.133
u	u	1	−2.133
$1-u$	$1-u$	0	−2.366
$1-u$	$1-u$	0	−2.366
$1-u$	$1-u$	−1	−2.133
$\frac{1}{2}-u$	$\frac{1}{2}+u$	$-\frac{1}{2}$	−2.133
$\frac{1}{2}+u$	$\frac{1}{2}-u$	$-\frac{1}{2}$	−2.133
u	u	−1	−2.133

Note. Oxygen removed from uuo, Ti_i moved to $-\frac{1}{2}00$, M^{3+} placed at $(-\frac{1}{2}00)$ and (-100).

TABLE IV

COORDINATES AND ELECTROSTATIC VALENCIES ESV OF OXYGEN IONS ASSOCIATED WITH RECONSTRUCTED VACANCY MODEL II (FIG. 4b)

Coordinates of oxygen ions experiencing changed esv			Σ esv of oxygen ions
$\frac{1}{2}-u$	$-\frac{1}{2}+u$	$\frac{1}{2}$	−1.333
$\frac{1}{2}-u$	$-\frac{1}{2}+u$	$-\frac{1}{2}$	−1.333
$-\frac{1}{2}+u$	$\frac{1}{2}-u$	$\frac{1}{2}$	−2.000
$-\frac{1}{2}+u$	$\frac{1}{2}-u$	$-\frac{1}{2}$	−2.000
$\bar{u}$	$\bar{u}$	0	−2.000
$-\frac{1}{2}-u$	$-\frac{1}{2}+u$	$\frac{1}{2}$	−2.666
$-\frac{1}{2}-u$	$-\frac{1}{2}+u$	$-\frac{1}{2}$	−2.666
$-1+u$	u	0	−2.666
$-1-u$	$-u$	0	−2.000
$-\frac{3}{2}+u$	$\frac{1}{2}+u$	$\frac{1}{2}$	−2.000
$-\frac{3}{2}+u$	$\frac{1}{2}-u$	$-\frac{1}{2}$	−2.000
$\frac{1}{2}+u$	$\frac{1}{2}-u$	$\frac{1}{2}$	−1.933
$\frac{1}{2}-u$	$\frac{1}{2}+u$	$\frac{1}{2}$	−1.933
$1-u$	$1-u$	1	−1.933
$1-u$	$1-u$	0	−1.933
			−1.866
$1-u$	$1-u$	0	−1.866
$1-u$	$1-u$	−1	−1.933
$\frac{1}{2}-u$	$\frac{1}{2}+u$	$-\frac{1}{2}$	−1.933
$\frac{1}{2}+u$	$\frac{1}{2}-u$	$-\frac{1}{2}$	−1.933
u	u	−1	−1.933

Note. Oxygen removed from (*uu0*) and $Ti_i(000)$ moved to $(-\frac{1}{2}00)$, M^{3+} placed at $(\frac{111}{222})$ and $(\frac{11}{22}-\bar{1})$.

(Model II, Fig. 4b). Thus M^{3+} ions may be placed in the symmetrically equivalent sites Ti_2 and Ti_3 (distorted five-coordination $[MO_5]$), whereas a Ti^{4+} interstitial is displaced from (000) to $(-\frac{1}{2}00)$, as before to share a face with a normal $[MO_6]$ octahedron at (−100) (Fig. 4b). *In this case the two M^{3+} ions have nearest neighbor oxygen vacancy and the Ti^{4+} interstitial has a second nearest neighbor oxygen vacancy.* The corresponding esv are analyzed in Table IV. Note that we are again left with two high values of −1.333, implying a lower energy for a H^+ associated with the vacancy. Otherwise the mean esv is −2.000 (since the defect overall is neutral). In this case

there appears to be an improvement in that six of the oxygens recover esv −2.000. However, this is counteracted by three oxygens taking esv = −2.666 instead of −2.333 and the last set of 10 oxygens listed take values greater, rather than less, than −2.000. Nevertheless, this distribution of Fe^{3+}, H^+, and Ti^{4+} ions is in excellent agreement with ESR results (see Section 4 below). The possibility that the ionization reaction $Fe^{3+} + e^- = Fe^{2+}$ may lead to Fe^{2+} ions in $[MO_6]$ or $[MO_5]$ sites should also be considered, but so far as we are aware there is no direct evidence for this.

Use of the $[MO_4]$ interstitial sites does not reduce the high esv = −1.333 values. Some redistributions of esv are achieved of course for the remaining oxygens but overall the values and distribution are similar to those listed in Tables I, III, and IV. Clearly, if four-coordination is acceptable for impurity atoms, then this may be more easily achieved by relaxation of the $[MO_5]$ sites adjacent to the oxygen vacancy. It is not considered worthwhile to provide here comprehensive lists of the esv derived for further possible reconstructions, including $[MO_4]$ and mixed $[MO_6]$ $[MO_4]$[3] distributions, except to say that we could find no experimental evidence for these from physical property measurements, in particular ESR studies (Section 3 below).

Similarly displacing two or even three of Ti_1, Ti_2, and Ti_3 simultaneously only further increases the number of oxygens having esv = −1.333. It is interesting to note however that if all three of these cations are displaced into regularly coordinated sites we are left with an almost regular void, having 12 vertices, centered on the oxygen vacancy (cf. the vacancy in a hcp array of ions). Such a defect could provide a nucleus for void or bubble formation and may become significant in irradiated rutiles.

It would appear from the above analysis that the traditional model may have lower electrostatic energy than the reconstructed models. A reconstruction containing only one face-shared pair of octahedral sites would appear attractive in view of its close structural relationship with the known structure of CSP in slightly reduced rutile. It is also the energetically favored arrangement in corundum-like structures M_2O_3 (M = Ti^{3+}, Al^{3+}, Cr^{3+}, and Fe^{3+}) and as such should lower the *chemical potential* of the defect, compensating for the higher electrostatic energy compared with the traditional vacancy model.

As described below incorporation of H^+ ions in the reconstructed defect should further stabilize the face-shared pair configuration. It is now necessary to develop improved defect energy calculation techniques for small defect complexes, along the lines of the HADES program (*15, 16*) in order to compare the traditional and reconstructed models. It is a weakness of the energy calculations so far that in obtaining relaxation energies the possibility of changes in the topology of coordination polyhedra was not included.

(*c*) *Diffusion mechanisms for oxygen vacancy defects.* For the traditional vacancy model diffusion is easily achieved by an adjacent oxygen ion jumping into the empty site. In reduced specimens charge neutrality may be maintained by accompanying jumps of electrons converting the corresponding Ti^{4+} ions into Ti^{3+} according to $Ti^{4+} + e^- = Ti^{3+}$. This reaction is believed to have low activation energy (*5, 6*). For doped specimens transport of M^{3+} cations *with* the traditional oxygen vacancy requires complex ring-like exchanges of Ti^{4+} and M^{3+} cations, probably utilizing the *c*-axis "tunnels" adjacent to the vacancy.

Diffusion of the reconstructed vacancy structure model I requires antiparallel jumps of oxygen ions (as above) and M^{3+}

[3] For example, Cu^{2+} may take square-planar four coordination (CuO) and Ga^{3+} is equally distributed over $[MO_6]$ and $[MO_4]$ sites in β-gallia (Ga_2O_3).

cations. One of the latter is already in the tunnel so its movement is relatively easy, the second M^{3+} ion requires a similar ring-type mechanism as for the traditional vacancy. For reconstructed model II diffusion is far easier, since all three cations Ti^{4+}, M^{3+} (×2) have parallel jumps, with a counterflow of O^{2-} ions jumping simultaneously into the vacancy. Of course if the activation energy for reactions like $Ti^{4+} + M^{3+} = Ti^{3+} + M^{4+}$ is not too great then the electrons originally (formally) attached to vacant oxygen sites will very quickly become delocalized. This is expected to be the normal situation for temperatures of ~room temperature and above (see, e.g., Refs. (*5, 6, 17*)). It is a matter for some concern that there exist no definitive studies of the detailed atomic and electronic mechanisms involved in diffusion of oxygen vacancies in nonstoichiometric rutiles. Clearly, from the above brief considerations and ESR results referred to below, differences may be expected between reduced and doped (or impure) specimens, and even between Fe^{3+} or Cr^{3+} doped specimens. There is a great need for development of techniques for determining directly the local electronic and atomic structural states of small defects.

3. Electron Spin Resonance Studies of Small Defects in Doped and Reduced Rutiles

In principle ESR studies offer a direct approach to the determination of small defect symmetries and electronic structure. However, as pointed out by Chester (*18, 19*), at absolute zero the defect in pure nonstoichiometric rutile must either be (according to a traditional viewpoint) an oxygen vacancy to which two electrons are bound, or an ionized interstitial titanium atom (Ti^{3+}). In either case the electron spin state must be $S = 0$ or $S = 1$. None of the more frequently observed spectra had $S = 1$ so it was concluded that the basic defect was *nonparamagnetic* and was therefore not detectable by ESR. It follows that the observed paramagnetic resonances must arise because of the transfer of electrons between the nonstoichiometric defects and impurities or other defects in the crystal, in order to leave unpaired electrons on some sites. Chester concluded with the prophetic statements:

(i) conductivity, infrared absorption, and ESR measurements on commercial crystals show that the defect structure of nonstoichiometric rutile is complex and depends on the impurities present;

(ii) in the absence of detailed knowledge the impurities present in each sample one cannot progress much further in understanding the observed behavior;

(iii) the evidence obtained favors the oxygen vacancy as the prime defect for small deviations from stoichiometry; and

(iv) hydrogen is shown to act as a *donor* and not just as a reducing agent.

Reduced and doped/reduced crystals of rutile become semiconducting, making it impossible to observe ESR spectra except for only very slight degrees of reduction (*20*). Conductivity absorbs microwave power and, even if the electron resonance is observed, it is characteristic of the band rather than the donor site; thus experiments are often carried out at liquid He temperatures. Even then only limited degrees of reduction may be studied. In fact the great majority of ESR studies of rutile must therefore have reference to the impurity controlled and O_V regimes II and III delineated by Marucco *et al.* (*5*), and referred to above.

Many ESR spectra of rutile have been reported and interpreted—mostly, at least prior to 1967, in terms of M^{n+} ions substituting for Ti^{4+} on octahedral sites. For critical reviews see the papers by Kerssen and Volger (*20*) and Andersson *et al.* (*21*) and references therein. In the remainder of this section we state the results of the higher

resolution ESR studies. We give here only the authors own firm conclusions. However, the literature is large, and often confusing, so that some readers may prefer to return to this section or to the original literature, after first reading the following section, where it is shown how our new structural models lead to a relatively straightforward clarification and understanding of the ESR results.

In 1967 improvements in spectrometer sensitivity led Miyako (*22*) to observe additional weak resonances which suggested that Co^{2+} ions are combined with a defect at the third neighbor O^{2-} sites, or (more probably) due to Co^{2+} ions combined with the oxygen vacancy at nearest neighbor O^{2-} sites. Later work (Miyako and Kazumata (*23*)) showed further complex weak spectra associated with the well-known substitutional Co^{2+} spectra. There were three groups of weak signals whose intensities could be varied by changing the degree of reduction. After a study of the symmetry of the resonance patterns and variations of signal intensity with degree of reduction, it was concluded that the three groups were associated with substitutional Co^{2+} in *combination* with nearest and second (or possibly third) nearest neighbor oxygen vacancies. It was also shown by Miyako that Co^{2+} was *also* associated with Ti^{4+} interstitial ions, as confirmed by ENDOR hyperfine interaction analysis (*24*).

Miyako *et al.* (*25*) then found two new weak paramagnetic signals in Cr^{3+}-doped rutiles. Analysis of both the directions of the symmetry axes and the magnitude of the spin Hamiltonian parameters led to the conclusion that these resonances come from substitutional Cr^{3+} spins coupled with second and third neighbor oxygen vacancies, respectively. The as-grown doped crystals were oxidized in air at 810°C for 210 hr, when all trace of the A-center reported by Chester was removed. The most remarkable feature of these new spectra was that the magnetic axes did not coincide with the axes of anion coordination polyhedra surrounding the substitutional site. It was argued that two Cr^{3+} ions substituted for Ti^{4+} would maintain charge neutrality for an oxygen vacancy, and the latter should remain near the Cr^{3+} ions because of the electrostatic affinity between them. The predicted magnetic axes for these two models give reasonable agreement with the observed symmetry axes.

In 1971 Meriaudeau *et al.* (*26*) reported the production of two types of paramagnetic centers in reduced rutiles (also anatase); the first being interpreted as substitutional and/or interstitial Ti^{3+}, and the second as Ti^{3+} in substitutional sites *but* combined with one or two oxygen vacancies.

Further weak spectra were studied by Kerssen and Volger (*20*) for rutiles doped with Al_2O_3 and subsequently given various degrees of reduction. At slight degrees of reduction (conductivity $\sigma \lesssim 10^{-2}\ \Omega^{-1}$, $T_r \lesssim$ 680°C) fourfold spectra were found (labeled B type) which were ascribed to electrons trapped at substitutional Ti^{4+} ions, near associates of a *substitutional and an interstitial* Al^{3+} ion. It was proposed that the first trapped electron creates the B-center: $Ti^{3+}(000)$–$Al^{3+}(0\frac{1}{2}0)$–Al^{3+} (010) and the second electron the B_{12} center: $Ti^{3+}(000)$–$Ti^{3+}(\pm\frac{1}{2}\frac{1}{2}\pm\frac{1}{2})$–$Al^{3+}(0\frac{1}{2}0)$–$Al^{3+}(010)$, where within the brackets the *approximate* sites are given. At higher degrees of reduction ($T_r \gtrsim 680$°C) the A-signal appeared, as first reported by Chester (*18*) and studied by many subsequent authors (see also comments below on paper by Shen *et al.* (*27*)). This signal and accompanying complicated hyperfine structure was only observed at $\lesssim$20 K. It was not explained satisfactorily, although the authors suggested tentatively that it may be due to hyperfine interactions of Ti^{3+} with substitutional Si^{4+} ions (a known impurity for their sample). A further signal (C-center) was also reported, again

this was interpreted tentatively as due to electrons trapped at oxygen vacancies, as suggested by the isotropic g-value and the small negative g-shift with respect to 2.0023. The fact that this resonance was rather broad indicated the unpaired electron wave function spread over neighboring Ti nuclei, which would give broadening due to unresolved hyperfine interactions with Ti nuclei. It was pointed out that Nowick and Heller (*28, 29*) had rigorously analyzed the results of anelastic-relaxation studies by Carnahan and Brittain (*30*) and by Wachtman *et al.* (*31, 32*) concluding that neither the traditional Ti^{3+} interstitial nor O^{2-} vacancy models were consistent with these experiments. Instead Nowick (*29*) suggested that a Ti interstitial should form a pair with some unspecified substitutional impurity located on a Ti^{4+} site.

Further ESR study of Al-doped rutile was reported by Zwingel (*33*). In single crystals ESR signals of holes were observed, trapped near $[Al]^-$ and $[Al–Al]^-$ centers upon ultraviolet excitation with the 405 Hg-line. The different centers could be thermally populated and quenched during warming of the crystals from liquid He[4] temperatures. Their charge state seemed to be related to charge transfer processes at other defect centers (presumed to be Fe^{3+} impurities).

Further evidence for small defect complexes in rutile followed the work of Andersson *et al.* (*21, 34*). Thus besides the well-known ESR spectrum of Fe^{3+} substitutional ions, three further spectra were recorded and interpreted by considering the intensity variation with heat treatment and the orientation of the magnetic axes of the extra spectra. In addition several other weak spectra were observed but could not be definitively interpreted. Spectrum I was interpreted as due to a substitutional Fe^{3+} ion which is perturbed by a nearby proton. If the Fe^{3+} ion is assumed to be at $(\frac{111}{222})$ the proton was shown to lie close to $(\frac{1}{2}00)$ (or equivalent) sites. Spectrum II was interpreted as due to a substitutional Fe^{3+} ion that is perturbed by a nearest neighbor oxygen vacancy. Several lines of spectrum III were identified and tentatively identified as due to a substitutional Fe^{3+} ion with a Ti^{4+} interstitial ion nearby.

It is especially interesting to note (*21*) that on annealing at a high temperature (1200°C) a substantial number of protons leave the crystal (study of spectrum I). Hence, a rapid cooling from 1200°C yielded crystals with a small content of protons.[4] On the other hand if the crystals were cooled very slowly (≅50°C/hr) protons were absorbed or trapped in the crystals. If the surrounding gas contained small amounts of hydrogen or water vapor, there was a net flow of protons *into* the crystal. Hence spectrum I was found to be more intense in annealed than in quenched crystals due to extra protons. For crystals annealed in an oxygen gas carefully cleaned of hydrogen and water vapor, few protons were left in the lattice irrespective of cooling rate and spectrum I was weak. Spectrum II was most intense in crystals rapidly cooled from 1200°C, since at this high temperature the crystal is in a reduced state. A slow cooling lowered the intensity of spectrum II, as expected for a center containing Fe^{3+} combined with oxygen vacancies.

In a further study of charge compensation mechanisms for Fe^{3+} in rutile Andersson *et al.* (*34*) determined the number of nearest neighbor oxygen vacancies, protons, and Ti^{4+} interstitials associated with Fe^{3+} substitutional ions. The first two of these followed from the ESR measurements. Since the number of ESR centers associated with oxygen vacancies was nearly the same as the number of oxygen vacancies it was concluded that the vacancies were predominantly located near iron

[4] Monitored by infrared studies of OH^- stretching frequencies.

ions. It was also shown that oxygen vacancies could only charge compensate for a fraction of the Fe^{3+} ions. Similarly, the number of protons calculated from the intensity of the OH line at 3286 cm^{-1} was insufficient for complete charge compensation. It was therefore suggested that the charge compensation in iron-doped rutile is mainly due to Ti^{4+} interstitial ions.[5]

Finally we refer to reinterpretation of Chester's A center by Shen *et al.* (*27*). A variety of rutiles were heated in atmospheres of H_2, H_2O, and O_2 according to prescriptions (*35, 36*) which theoretically and experimentally favor or suppress (respectively) H^+ interstitial formation. The OH concentration and conduction electron concentrations were monitored optically. It was established reasonably convincingly that the A spectrum was associated with protons. (A typical treatment leading to the A spectrum would be 800°C for 10 hr in an atmosphere of <1 Torr. O_2 or H_2 and 18 Torr of H_2O.) It was concluded that since the A spectrum is highly correlated with H^+ ions then it cannot arise from Ti^{3+} interstitials or oxygen vacancies, etc. Clearly this last is an extreme oversimplification. A more complex defect, such as our reconstructed model I, which includes OH^- associated with an oxygen vacancy, a substitutional Ti^{3+} *and* a Ti^{3+} interstitial, is quite consistent with the optical studies of Shen *et al.* (see also discussion of Ref. (*26*)). Positive location of the proton was not achieved by Shen *et al.*, due to the weakness of hyperfine interaction spectra, but it was claimed that it was also approx. at $(\frac{1}{2}00)$. Different weak signals, due to centers resulting from reduction in dry hydrogen, were not analyzed in detail.

[5] We note here that in our model II each oxygen (and H^+) may be associated with *two* Fe^{3+} ions, obviating the necessity to invoke a further impurity and offering a reasonable mechanism to balance these bookkeeping problems.

4. Discussion

(*a*) *Comparison of Predicted Oxygen Vacancy Structures (Reconstructed Models I and II) with ESR Results*

It is clear from Section 3 above that our reconstructed models I and II offer new insight into the results of ESR analyses. The traditional oxygen vacancy and titanium interstitial models are certainly not valid. The results for Cr^{3+}, Al^{3+}, Fe^{3+}, and Co^{2+} are very important. In each case a defect complex is implied by ESR spectra.

For Cr^{3+} the ESR model requires substitutional Cr^{3+} spins coupled with second and third neighbor oxygen vacancies, respectively. In our model I this would correspond to Cr^{3+} at $(-\frac{1}{2}00)$ and (-100), with oxygen vacancy at $(uu0)$. Note that only (-100) is strictly substitutional, $(-\frac{1}{2}00)$ is certainly octahedral but displaced into an interstitial site. This is not, however, the traditional interstitial, since it leaves vacant a normal site at (000). Thus the immediate environment retains many of the features of a substitutional site. Inspection of a model of reconstruction I shows that the magnetic axes for Cr^{3+} at (-100) with respect to an oxygen at $(uu0)$ are identical with the model proposed in Ref. (*24*) for the third nearest neighbor, whereas those for Cr^{3+} at $(-\frac{1}{2}00)$ change by ~5° from the axes proposed for the second nearest neighbor. Thus our model offers a reasonable alternative explanation for the ESR result. A more detailed ESR analysis should be carried through, based upon model I, but this is beyond our expertise.

For Fe^{3+} the three spectra additional to the strong spectra from substitutional Fe^{3+} required Fe^{3+} interaction with (i) H^+ (at $\cong(\frac{1}{2}00)$ for Fe^{3+} at $(\frac{111}{222})$); (ii) Fe^{3+} adjacent to a nearest neighbor oxygen vacancy (say $(uu0)$); and (iii) a Fe^{3+} ion with a Ti^{4+} interstitial ion nearby. Clearly all three of these geometries are immediately and precisely predicted by our reconstructed model II.

As pointed out by Andersson *et al.* (*21*) the different ESR spectra obtained for Fe^{3+}- and Cr^{3+}-doped rutiles support the results of crystal field calculations for these ions with high- and low-spin octahedral coordinations subjected to distortions (*37*). The latter showed that for removal of a ligand, the total energy of a Fe^{3+} ion remains constant, whereas that of a Cr^{3+} ion increases. Thus Fe^{3+} may occupy the distorted $[MO_5]$ coordinated sites adjacent to the vacancy (our model II) whereas Cr^{3+} require octahedral coordination as is achieved in our model I.

For Al^{3+} the ESR results clearly require a pairing of Al^{3+}–Al^{3+} ions in adjacent octahedral sites. Thus both the B and B_{12} centers (*20*) contain face-shared octahedral pairs of Al^{3+} at $(0\frac{1}{2}0)$ and (010), symmetrically equivalent to the face-shared pair at (−100), $(-\frac{1}{2}00)$ in our model I. However, Kerssen and Volger (*20*) place the nearby Ti ions in normal octahedral sites, leading to strings of three-face sharing (e.g., $Ti^{3+}(000)$–$Al^{3+}(0\frac{1}{2}0)$–$Al^{3+}(010)$ for the B center). In our model I (after an axial transformation) we have $Al(0\frac{1}{2}0)$–Al(010) but there is no ion at (000). Careful reading of Ref. (*20*) shows that there is no direct evidence for a Ti^{3+} ion at (000). It is merely a convenient place at which to "trap an electron"; however, Ti^{3+} at $(\frac{111}{222})$ would serve equally as far as their model is concerned, as there is no ESR signal from the Ti^{3+} ion itself. The reason why Kerssen and Volger require this associated Ti ion to have charge 3+ rather than 4+ seems to us to be somewhat obscure, since it is not required for charge compensation nor do they indicate the position of the oxygen vacancy with respect to the $Al(0\frac{1}{2}0)$–Al(010) pairing. Again we suggest that further detailed analysis of the observed hyperfine splittings and magnetic axes should be carried through on the basis of our model I. A detailed comparison of the spectra from Fe^{3+} and Al^{3+}, and a search for H^+ in $Al:TiO_2$ should be attempted.

For Co^{2+} ESR centers were proposed (*23*) requiring Co^{2+} in substitutional sites in combination with nearest and second nearest neighbor oxygen vacancy sites. Co^{2+} was also associated with a Ti^{4+} interstitial site. This arrangement is closely approximated by a modification to our models I and II whereby one Co^{2+} is placed at, e.g. $(\frac{111}{222})$, as is the case for Fe^{3+} in model II, with a nearest neighbor oxygen vacancy, whereas a second Co^{2+} ion is placed at (−100), as in model I. The latter is a substitutional site, but has the oxygen vacancy as a third nearest neighbor, rather than second. The Ti^{4+} interstitial site would be $(-\frac{1}{2}00)$. We note that in his first paper Miyako (*22*) stated that the spectra are possible to explain for Co^{2+} associated with nearest and third nearest oxygen vacancy sites, in agreement with our assignment $Co^{2+}(-100)$–$Ti^{4+}(-\frac{1}{2}00)$–$Co^{2+}(\frac{111}{222})$. In the later paper (*23*) Co^{2+} is preferred at second nearest neighbor distance from the vacancy. However, the agreement between observed and assigned magnetic axes is again only approximate, and probably not definitive, at least until the spectra have been analyzed again to test sensitiveness to our proposed models. Clearly the geometry we propose overlaps considerably with that proposed by Miyako, with subtle differences which were not tested by his analysis.

The ESR spectra of reduced rutile powders (*26*) is especially interesting, since rutile powders are obtainable having significantly higher purity than was the case for single crystal rutile boules. Two resonance centers were recorded and identified; the first containing Ti^{3+} ions on normal lattice sites and/or on interstitial sites whereas the second contained Ti^{3+} ions on normal sites associated with one or two vacant oxygen sites. These results are readily consistent with model I where we have Ti^{3+} at (−100),

a normal lattice site and Ti^{3+} at $(-\frac{1}{2}00)$, an interstitial site; with the oxygen vacancy nearby. Again it is necessary to reanalyze each ESR spectra using model I, since it appears to offer a natural explanation for both spectra. In view of the results of Andersson *et al.* (*21*) for Fe : TiO_2 and of Shen *et al.* (*27*) for reduced TiO_{2-x} a careful search for H^+ ions associated with ESR centers in reduced *pure* rutiles should be made, since the trapping of H^+ in the vicinity of vacant oxygen sites is predicted by our models I and II.

It should be stated here that models I and II (and the permutation referred to in discussing the case of Co^{2+} : TiO_2) do not exhaust the possibilities for reconstructed oxygen vacancy structures. Thus there may be some tendency for the face-shared pair of octahedra to become further separated from the vacancy (using a Frenkel defect diffusion mechanism, e.g., with (−100) displaced to $(-\frac{3}{2}00)$, forming a new face-shared pair $M^{3+}(-200)$–$M^{3+}(-\frac{3}{2}00)$. Similarly at sufficiently high temperatures, or on quenching from such temperatures, H^+ ions may become detached from the favorable trapping site at the oxygen vacancy. Further variations may be envisaged if reactions such as

$$M^{3+} + Ti^{4+} \rightarrow M^{4+} + Ti^{3+}$$

are favored under some preparation conditions, so that, e.g., Cr^{4+} may reasonably enter substitutional sites and Ti^{3+} shift to face-shared octahedral sites. Ga^{3+} occupies $[MO_4]$ octahedral sites in β-Ga_2O_3 and in gallia-doped rutiles (*38*). ESR spectra of Ga : TiO_2 may reveal further new paramagnetic resonance phenomena. The possibility of Cu^{2+} or Ni^{2+} taking square planar four-coordination adjacent to an oxygen vacancy should also be investigated.

We conclude this section by noting that it is remarkable that the relatively very simple modifications of the traditional vacancy model proposed here (essentially *one* cation is displaced from (000) to $(-\frac{1}{2}00)$) have been surprisingly successful in apparently rationalizing many puzzling observations from a rather large number of ESR studies. Clearly further detailed ESR work is required to test and extend these models.

(*b*) *Relationship of Reconstructed Vacancy Models to Results of Other Physical Property Measurements*

There are large numbers of papers existing in the literature relating to physical property measurements of rutile. It has only recently been established clearly (*5, 6*) that there may be three different regimes of predominant small defect behaviors within the TiO_{2-x} phase (see Ref. (*5*), Fig. 3). Thus it is extremely difficult to concisely summarize and correlate results from, e.g., Ti and O atom diffusivity measurements (see, e.g., Refs. (*1, 38–40*) and Refs. therein), thermogramimetric and electrical conductivity studies ((*2, 3, 5, 6, 42*) and Refs. therein), dielectric and anelastic relaxation (*28–32, 43*), thermoelectric power (*44, 45*), and proton channeling experiments (*45*). In many cases impurity contents were not controlled, and a wide variety of methods of reduction (heating *in vacuo,* heating in H_2/H_2O or CO/CO_2 gas buffers heating in dry hydrogen, etc.) were used. Overall on reading these (and many other papers) a picture emerges which is consistent with the "phase diagram" of Marucco *et al.* (*5*), and the new defect models derived here and in Ref. (*11*). Thus oxygen vacancy defects predominate at relatively high partial pressures of oxygen, these are often required to be associated with interstitial M^{3+} or M^{4+} ions, and are favored if the reduction technique does not specifically exclude H_2O (*47*). For larger degrees of reduction titanium interstitial defects are favored, i.e., relatively low partial pressures of oxygen. The new defect models derived in this pa-

per for oxygen vacancy defects and in (*11*) for interstitial defects offer convincing structural explanations for many of the confusing results reported, especially in the earlier literature (say, 1959–1977). Thus many specimens studied certainly contained both impurity controlled oxygen vacancy defects, which *themselves* contain associated [MO_6 *interstitial* sites (our reconstructed models I and II above), in addition to linear interstitial defects (*11*) containing two pairs of face-shared octahedra. Clearly the principles of point-defect equilibria (see, e.g., Kofstad (*2*)) need to be modified to account for both linear interstitial defects and the reconstructed oxygen vacancy complexes if any further progress is to be made in the interpretation of many physical property bulk measurements. In a separate paper it is shown that appropriate modifications to the theoretical basis for small defect equilibria analysis may be made, using complexes rather than individual point defects, which yield results, e.g., for log σ versus $1/T$, etc., which are in agreement with experimental results.

(*c*) *Aggregation of Small Defects*

At some stage in a reduction process, or on increasing dopant levels sufficiently, or on cooling reduced or doped specimens sufficiently slowly across the TiO_{2-x} phase boundary, oxygen vacancy defects, and/or interstitial defects are likely to interact together to precipitate as CSP. Aggregation and precipitation of CSP in the interstitial regime I has been thoroughly studied by high-resolution electron microscopy (*7–10*). Pairs of CSP and also platelet defects were observed which were readily explained using the linear cationic interstitial models (*11*). So far few of the many specimens examined by HREM have been cooled from the narrow stoichiometry range TiO_{2-x} ($0 \lesssim x \lesssim 0.0016$) corresponding to the oxygen vacancy regime. However, we expect to eventually find evidence for a vacancy loop mechanism in this regime.

(*d*) *Direct Imaging of Small Defect Structures*

The first HREM images showing evidence for small defects in quenched $TiO_{1.9985,1.9966}$ specimens were published recently (*8*) and computer simulations of the image contrast (*48*) show that it will be possible to directly image, and positively identify, such small defects as proposed here and in (*11*) under very specific imaging conditions. *In situ* studies of the precipitation and dissolution of CSP, and complementary HREM studies, have already produced positive results and are in the course of publication (*8, 49*).

(*e*) *Interaction between Small Defects and Dislocations*

Much of the original impetus for the present work arose during studies of the plastic deformation of rutile single crystals (*50*). Dynamic strain ageing studies revealed two small defect types interacting with dislocations belonging to the slip system $\{101\}\langle 10\bar{1}\rangle$. It is now reasonable to assume that at least one of these will be an impurity (probably Al^{3+})-controlled oxygen vacancy defect. Clearly we are hopeful that the interaction of small defects with extended defects, such as dislocations and CSP, will be directly observable by *in situ* HREM studies before very long, as such an experimental technique seems to be required in order to fully expose the nature of small defect/extended defect equilibria.

Acknowledgments

This work was supported financially by the University of Melbourne and the Australian Research Grants Committee. L. A. Bursill is grateful to the University of Lyon for support of a visit to Lyon in 1982.

References

1. J. R. Akse and H. B. Whitehurst, *J. Phys. Chem. Solids* **39,** 451 (1978).
2. P. Kofstad, "Non-stoichiometry, Diffusion, and Electrical Conductivity in Binary Metal Oxides," pp. 22 and 137, Wiley–Interscience, New York (1972).
3. J. F. Baumard, D. Panis, and A. M. Anthony, *J. Solid State Chem.* **7,** 177 (1972).
4. M. G. Blanchin, P. Faisant, C. Picard, M. Ezzo, and G. Fontaine, *Phys. Status Solidi A* **60,** 357 (1980).
5. J. F. Marucco, J. Gautron, and P. Lemasson, *J. Phys. Chem. Solids* **42,** 363 (1981).
6. J. Gautron, J. F. Marucco, and P. Lemasson, *Mater. Res. Bull.* **16,** 515 (1981).
7. L. A. Bursill, M. G. Blanchin, and D. J. Smith, *Proc. Roy. Soc. (London) A* **384,** 135 (1982).
8. L. A. Bursill, M. G. Blanchin, A. Mabarek, and D. J. Smith, *Radiat. Eff.*, in press.
9. M. G. Blanchin, L. A. Bursill, and D. J. Smith, *Proc. Roy. Soc. (London)*, in press.
10. L. A. Bursill, M. G. Blanchin, and D. J. Smith, *Proc. Roy. Soc. (London)*, in press.
11. H. D. Megaw, "Crystal Structures: a Working Approach," p. 39, Saunders, New York, (1973).
12. L. A. Bursill and M. G. Blanchin, *J. Phys. (Lett.)* **44,** L165 (1983).
13. L. A. Bursill and B. G. Hyde, *Progr. Solid State Chem.* **7,** 177 (1972).
14. J. S. Anderson and B. G. Hyde, *J. Phys. Chem. Solids* **28,** 1393 (1967).
15. C. R. A. Catlow and R. James, *Proc. Roy. Soc. (London) A* **384,** 152 (1982).
16. C. R. A. Catlow, R. James, W. C. Mackrodt, and R. F. Stewart, *Phys. Rev. B* **25,** 1006 (1982).
17. C. Schlenker and M. Marezio, *Philos. Mag. B* **42,** 453 (1980).
18. P. F. Chester, *J. Appl. Phys.* **32,** 2233 (1961).
19. P. F. Chester, J. Holt, B. J. Maddock, and A. B. Willott, Central Electricity Research Laboratories Report No. RD/L/R-1267, Leatherhead, England, 1964 (unpublished).
20. J. Kerssen, and J. Volger, *Physica* **69,** 535 (1973).
21. P.-O. Andersson, E. L. Kollberg, and A. Jelenski, *Phys. Rev. B* **8,** 4956 (1973).
22. Y. Miyako, *Phys. Lett. A* **24,** 635 (1967).
23. Y. Miyako and Y. Kazumata, *J. Phys. Soc. Jpn.* **31,** 1727 (1971).
24. Y. Miyako, *J. Phys. Soc. Jpn.* **31,** 1732 (1971).
25. M. Ikebe, Y. Miyako, and M. Date, *J. Phys. Soc. Jpn.* **26,** 43 (1969).
26. P. Meriaudeau, M. Che, P. C. Gravelle, and S. J. Teichner, *Bull.-Soc. Chim. Fr.* pp. 13 (1971).
27. L. N. Shen, O. W. Johnson, W. D. Ohlsen, and J. W. DeFord, *Phys. Rev. B* **10,** 1823 (1974).
28. A. S. Nowick and W. R. Heller, *Advan. Phys.* **14,** 101 (1965).
29. A. S. Nowick, *Advan. Phys.* **16,** 1 (1967).
30. R. D. Carnahan and J. O. Brittain, *J. Appl. Phys.* **34,** 3095 (1963).
31. J. B. Wachtman (Jr.) and L. R. Doyle, *Phys. Rev. A* **135,** 276 (1964).
32. J. B. Wachtman (Jr.), S. Spinner, W. S. Brower, T. Fridinger, and R. W. Dickson, *Phys. Rev.* **148,** 811 (1966).
33. D. Zwingel, *Solid State Commun.* **20,** 397 (1976).
34. P. O. Andersson, E. L. Kollberg, and A. Jelenski, *J. Phys. C: Solid State Phys.* **7,** 1868 (1974).
35. J. W. Deford and O. W. Johnson, *J. Appl. Phys.* **44,** 3001 (1973).
36. O. W. Johnson, J. DeFord, and J. W. Shaner, *J. Appl. Phys.* **44,** 3008 (1973).
37. H. L. Schläfer and G. Gliemann, Einfürung in die Liegandfeldttheorie (Akademische Verlagsgesellschaft, Frankfurt au Main, 1967).
38. G. G. Stone and L. A. Bursill, *Philos. Mag.* **35,** 1397 (1977).
39. D. A. Venkatu and L. E. Poteat, *Mater. Sci. Eng.* **5,** 258 (1969/70).
40. J. F. Baumard, *Solid State Commun.* **20,** 859 (1976).
41. E. Iguchi and K. Yajima, *J. Phys. Soc. Jpn.* **32,** 1415 (1972).
42. V. N. Bogomolov, I. A. Smirnov, and E. V. Shadrickev, *Sov. Phys. Solid State* **11,** 2606 (1970).
43. L. A. K. Daminik and R. K. MacCrone, *Phys. Rev.* **163,** 756 (1967).
44. J. F. Baumard and E. Tani, *Phys. Status Solidi A* **39,** 373 (1977).
45. J. Yahia, *Phys. Rev.* **130,** 1711 (1963).
46. E. Yagi, A. Koyama, H. Sakawi, and R. R. Hasiguti, *J. Phys. Soc. Jpn.* **42,** 939 (1977).
47. R. D. Shannon, *J. Appl. Phys.* **35,** 3414 (1964).
48. L. A. Bursill and Shen Gwang Jun, submitted for publication.
49. L. A. Bursill, M. G. Blanchin, and D. J. Smith, in preparation.
50. M. G. Blanchin, G. Fontaine, and L. P. Kubin, *Philos. Mag.* **41,** 261 (1980).